

Meson Masses and Mixing Angles in 2+1 Flavor Polyakov Quark Meson Sigma Model and Symmetry Restoration Effects

Uma Shankar Gupta* and Vivek Kumar Tiwari†

Department of Physics, University of Allahabad, Allahabad 211002, India.

(Dated: February 17, 2019)

The meson masses and mixing angles have been calculated for the scalar and pseudoscalar sector in the framework of generalized 2 + 1 flavor Polyakov loop augmented Quark Meson Linear Sigma (PQMS) Model. We have given the results for two different forms of effective Polyakov loop potential. The comparison of results with the existing calculations in the bare 2+1 Quark Meson Linear Sigma (QMS) Model, shows that the restoration of chiral symmetry becomes sharper due to the influence of the Polyakov loop potential. We find that inclusion of Polyakov loop in QMS model together with the presence of axial anomaly, triggers an early and significant melting of the strange condensate. We have examined how the inclusion of Polyakov loop qualitatively and quantitatively affects the convergence in the masses of the chiral partners in pseudoscalar (π , η , η' , K) and scalar (σ , a_0 , f_0 , κ) meson nonets as the temperature is varied on the reduced temperature scale. The role of $U_A(1)$ anomaly in determining the isoscalar masses and mixing angles for the pseudoscalar (η and η') and scalar (σ and f_0) meson complex, has also been investigated in the PQMS model. The interplay of chiral symmetry restoration effects and the setting up of $U_A(1)$ restoration trend has been discussed and analyzed in the framework of the presented model calculations.

PACS numbers: 12.38.Aw, 11.30.Rd, 12.39.Fe, 11.10.Wx

I. INTRODUCTION

The present theoretical understanding of strong interaction physics indicates that normal hadronic matter undergoes a phase transition, where the individual hadrons dissolve into their constituents and produce a collective form of matter known as the Quark Gluon plasma (QGP) under the extreme conditions of high temperature and/or density [1, 2, 3]. Relativistic heavy ion collision experiments at RHIC (BNL), LHC (CERN) and the future CBM experiments at the FAIR facility (GSI-Darmstadt) aim to create and study such a collective state of matter.

Study of the different aspects of this phase transition, is a tough and challenging task because Quantum Chromodynamics (QCD), the theory of strong interaction, becomes nonperturbative in the low energy limit. In the zero quark mass limit, chiral condensate works as an order parameter for the spontaneous breakdown of the chiral symmetry in the low energy hadronic vacuum of the QCD. For the infinitely heavy quarks, in the pure gauge $SU_c(3)$ QCD, the $Z(3)$ (Centre symmetry of the QCD color gauge group) symmetry, which is the symmetry of hadronic vacuum, gets spontaneously broken in the high temperature/density regime of QGP. Here the expectation value of the Wilson line (Polyakov loop) is related to the free energy of a static color charge, hence it serves as the order parameter of the confinement-deconfinement phase transition [4].

Even though the centre symmetry is always broken with the inclusion of dynamical quarks in the system, one can regard the Polyakov loop as an approximate order parameter because it is a good indicator of the confinement-deconfinement transition [5, 6].

We get important information and insights from the lattice QCD calculations [7, 8, 9, 10, 11, 12, 13, 14] regarding various aspects of the transition, like the restoration of chiral symmetry in QCD, order of the confinement/deconfinement phase transition, richness of the QCD phase structure and mapping of the phase diagram. Since lattice calculations are technically involved and various issues are not conclusively settled within the lattice community, one resorts to the calculations within the ambit of phenomenological models developed in terms of effective degrees of freedom. These models serve to complement the lattice simulations and give much needed insight about the regions of phase diagram inaccessible to lattice simulations. Lot of current effective model building activity, is centred around combining the features of spontaneous breakdown of both chiral symmetry as well as the centre $Z(3)$ symmetry of QCD in one single model [15, 16, 17, 18, 19, 20, 21, 22, 23, 24, 25, 26, 27, 28, 29]. In these models chiral condensate and Polyakov loop are simultaneously coupled to the quark degrees of freedom.

In order to calculate the properties of mesons in hot and dense medium, several investigations have been done in the two/three flavor NJL, PNJL models [30, 31, 32, 33] and also in the $SU(2)$ version of linear sigma model [34, 35, 36]. Since chiral symmetry restoration is signaled by parity doubling, these studies look for the pattern of emerging convergence in the masses of the chiral partners in pseudoscalar (π , η , η' , K) and scalar mesons (σ ,

*Electronic address: guptaung@gmail.com

†Electronic address: vivekkr@gmail.com

a_0, f_0, κ). It is a common knowledge that the basic QCD lagrangian has the $SU_{L+R}(3) \times SU_{L-R}(3) \times U_A(1)$ symmetry. Different patterns of spontaneous as well as explicit beaking of $SU_V(3) \times SU_A(3)$, have been discussed by Lenaghan et al. [37] in the ambit of $SU(3)$ Linear Sigma model. Schaefer et al. enlarged the Linear Sigma Model with the inclusion of quarks [41] and then they studied in the 2+1 flavor breaking scenario, the consequences of $SU(3)$ chiral symmetry restoration for scalar and pseudo scalar meson masses and mixing angles, in the presence as well as the absence of $U_A(1)$ axial symmetry, as the temperature is increased through the phase transition temperature. The $U_A(1)$ axial symmetry does not exist at the quantum level and as shown by 'tHooft [38] it gets explicitly broken to $Z_f(3)$ by the instanton effects. This $U_A(1)$ anomaly does not let the η' meson remain massless goldstone boson in the chiral limit by giving it a mass of about 1 GeV and further it also leads to flavor mixing, a phenomenon that lifts the degeneracy between the π and η' which otherwise would have been degenerate with π in $U(3)$ even if the explicit chiral symmetry breaking is present. There is large violation in Okubo-Zweig-Iizuka [OZI] rule for both pseudoscalar and scalar mesons and ideal mixing is not achieved because of strong flavor mixing between nonstrange and strange flavor components of the mesons [31]. Hence $U_A(1)$ restoration will have important observable effects on scalar pseudoscalar meson masses as well as the mixing angles.

In a three flavor PNJL model calculation, Costa and collaborators [31] have discussed in detail how the inclusion of Polyakov loop in the NJL model, affects the results of meson mass and mixing angle calculations. However they have pointed out that the description of the η' in the NJL model has some problem [32]. The NJL model does not confine and the meson degrees of freedom are generated in the model by some prescription. The polarization function for the meson gets an imaginary part above the $\bar{q}q$ threshold, hence η' becomes unbound completely in the model soon after the temperature is raised from zero. Thus η' in the NJL model is not a well defined quantity [39]. Schaefer et al [40, 41]. have also made an elaborate study of meson masses and mixing angles with and without $U_A(1)$ axial anomaly in the 2+1 flavor, Quark Meson Linear Sigma Model where the mesons are included in the lagrangian from the very outset and the $U_A(1)$ breaking 'tHooft coupling term is constant. The behaviour of the scalar and pseudoscalar mixing angles in their calculation is opposite to what has been reported in the calculation by Costa et. al. [31]. It is worthwhile and important to investigate the influence of Polyakov loop on meson mass and mixing angle calculations, in scalar and pseudoscalar sector, in the framework of generalized 2+1 flavor Quark Meson Linear Sigma Model enlarged with the inclusion of Polyakov loop [15]. Since we are lacking in the experimental information on the behaviour of mass and mixing angle observables in the medium, a comparative study of

these quantities in different models and circumstances becomes all the more desirable. We will be investigating how the inclusion of Polyakov loop, qualitatively and quantitatively affects the convergence of the masses of chiral partners, when the parity doubling takes place as the temperature is increased through T_c and the partial restoration of chiral symmetry is achieved. We will also be studying the effect of Polyakov loop on the interplay of $SU_A(3)$ chiral symmetry and $U_A(1)$ symmetry restoration.

The arrangement of this paper is as follows. In Sec.II we have given the formulation of the model. The description of grand potential in the mean field approach has been presented in Sec.III. We have derived the modification of meson masses due to the $\bar{q}q$ contribution in the presence of Polyakov loop in Sec.IV, which discusses meson masses and mixing angles. In Sec.V we will be discussing the numerical results and plots, for understanding and analysing the effect of Polyakov loop on chiral symmetry restoration.

II. MODEL FORMULATION

We will be working in the generalized three flavor Quark Meson chiral Linear Sigma Model which has been combined with the Polyakov loop potential [15, 40, 41, 42]. In this model quarks coming in three flavor are coupled to the $SU_V(3) \times SU_A(3)$ symmetric mesonic fields together with spatially constant temporal gauge field represented by Polyakov loop potential. Polyakov loop field $\Phi(\vec{x})$ is defined as the thermal expectation value of color trace of Wilson loop in temporal direction

$$\Phi = \frac{1}{N_c} \text{Tr}_c L, \quad \Phi^* = \frac{1}{N_c} \text{Tr}_c L^\dagger \quad (1)$$

where $L(x)$ is a matrix in the fundamental representation of the $SU_c(3)$ color gauge group.

$$L(\vec{x}) = \mathcal{P} \exp \left[i \int_0^\beta d\tau A_0(\vec{x}, \tau) \right] \quad (2)$$

Here \mathcal{P} is path ordering, A_0 is the temporal vector field and $\beta = T^{-1}$ [4].

The model Lagrangian is written in terms of quarks, mesons, couplings and Polyakov loop potential $\mathcal{U}(\Phi, \Phi^* T)$.

$$\mathcal{L}_{PQMS} = \mathcal{L}_{QMS} - \mathcal{U}(\Phi, \Phi^*, T) \quad (3)$$

$$\mathcal{L}_{QMS} = \bar{q}_f (i\gamma^\mu D_\mu - g T_a (\sigma_a + i\gamma_5 \pi_a)) q_f + \mathcal{L}_m \quad (4)$$

The coupling of quarks with the uniform temporal background gauge field is effected by the following replacement $D_\mu = \partial_\mu - iA_\mu$ and $A_\mu = \delta_{\mu 0} A_0$ (Polyakov

gauge), where $A_\mu = g_s A_\mu^a \lambda^a / 2$. g_s is $SU_c(3)$ gauge coupling. λ_a are Gell-Mann matrices in the color space, a runs from $1 \cdots 8$. $q_f = (u, d, s)^T$ denotes the quarks coming in three flavors and three colors. g is the flavor blind Yukawa coupling that couples the three flavor of quarks with nine mesons in the scalar ($\sigma_a, J^P = 0^+$) and pseudoscalar ($\pi_a, J^P = 0^-$) sectors.

The quarks have no intrinsic mass but become massive after spontaneous chiral symmetry breaking because of nonvanishing vacuum expectation value of the chiral condensate. The mesonic part of the lagrangian has the following form

$$\begin{aligned} \mathcal{L}_m = & \text{Tr}(\partial_\mu M^\dagger \partial^\mu M) - m^2 \text{Tr}(M^\dagger M) - \lambda_1 [\text{Tr}(M^\dagger M)]^2 \\ & - \lambda_2 \text{Tr}(M^\dagger M)^2 + c[\det(M) + \det(M^\dagger)] \\ & + \text{Tr}[H(M + M^\dagger)]. \end{aligned} \quad (5)$$

The chiral field M is a 3×3 complex matrix comprising of the nine scalars σ_a and the nine pseudoscalar π_a mesons.

$$M = T_a \xi_a = T_a(\sigma_a + i\pi_a) \quad (6)$$

Here T_a represent 9 generator of $U(3)$ with $T_a = \frac{\lambda_a}{2}$. $a = 0, 1 \dots 8$. λ_a are standard Gell-Mann matrices with $\lambda_0 = \sqrt{\frac{2}{3}} \mathbf{1}$. The generators follow $U(3)$ algebra $[T_a, T_b] = if_{abc} T_c$ and $\{T_a, T_b\} = d_{abc} T_c$ where f_{abc} and d_{abc} are standard antisymmetric and symmetric structure constants respectively with $f_{ab0} = 0$ and $d_{ab0} = \sqrt{\frac{2}{3}} \mathbf{1} \delta_{ab}$ and Matrices are normalized as $\text{Tr}(T_a T_b) = \frac{\delta_{ab}}{2}$.

The $SU_L(3) \times SU_R(3)$ chiral symmetry is explicitly broken by the explicit symmetry breaking term

$$H = T_a h_a \quad (7)$$

Here H is a 3×3 matrix with nine external parameters.

The ξ field picks up the nonzero vacuum expectation value, ξ due to the spontaneous breakdown of the chiral symmetry. Since ξ must have the quantum numbers of the vacuum, explicit breakdown the chiral symmetry is only possible with three nonzero parameters h_0 , h_3 and h_8 . We are neglecting isospin symmetry breaking hence we choose $h_0, h_8 \neq 0$. This leads to the $2 + 1$ flavor symmetry breaking scenario with nonzero condensates $\bar{\sigma}_0$ and $\bar{\sigma}_8$.

Apart from h_0 and h_8 the other parameters in the model are five in number. These are the squared tree-level mass of the meson fields m^2 , quartic coupling constants λ_1 and λ_2 , a Yukawa coupling g and a cubic coupling constant c which models the $U_A(1)$ axial anomaly of the QCD vacuum.

The $U_A(1)$ axial is anomalous and it is broken by the quantum effects [46]. In the absence of $U_A(1)$ anomaly η' meson would have been ninth light pseudoscalar goldstone boson, resulting due to the spontaneous break down of the chiral $U_A(3)$ symmetry. The entire pseudoscalar nonet corresponding to spontaneously

broken $U_A(3)$, consists of three π , four K , η and η' mesons. In order to study the chiral symmetry restoration at high temperatures, we will be investigating the trend of convergence in the masses of chiral partners occurring in pseudoscalar (π, η, η', K) and scalar (σ, a_0, f_0, κ) nonets, in the $2 + 1$ flavor symmetry breaking scenario.

A. Choice of Potentials for the Polyakov Loop

The effective potential $\mathcal{U}(\Phi, \Phi^*, T)$ is constructed such that it reproduces thermodynamics of pure glue theory on the lattice for temperature upto about twice of deconfinement phase transition temperature. At much higher temperature the transverse gluons become effective degrees of freedom, hence the construction of effective potential in terms of the Polyakov loop potential is not reliable [18, 30].

At low temperatures, in confined phase the effective potential U has only one minimum at $\Phi = 0$. Above the critical temperature for deconfinement transition, $\Phi = 0$ becomes metastable local minima and now, the effective potential has three degenerate global minima at $\Phi \neq 0$.

In this work, we use the following two choices of the effective potential. The first which is based on Polyakov loop polynomial expansion was proposed in Ref [18].

$$\begin{aligned} \frac{\mathcal{U}_{\text{pol}}(\Phi, \Phi^*, T)}{T^4} = & -\frac{b_2}{4} (|\Phi|^2 + |\Phi^*|^2) - \frac{b_3}{6} (\Phi^3 + \Phi^{*3}) \\ & + \frac{b_4}{16} (|\Phi|^2 + |\Phi^*|^2)^2 \end{aligned} \quad (8)$$

The second term that is sum of Φ^3 and Φ^{*3} terms, causes the three degenerate vacua above the deconfinement phase transition. Consequently the potential has the $Z(3)$ symmetry in the confined phase. The potential parameters are adjusted according to the pure lattice data such that the equation of state and Polyakov loop expectation values are reproduced. The temperature dependent coefficient $b_2(T)$ governs the confinement - deconfinement phase transition and is given by

$$b_2(T) = a_0 + a_1 \left(\frac{T_0}{T}\right) + a_2 \left(\frac{T_0}{T}\right)^2 + a_3 \left(\frac{T_0}{T}\right)^3.$$

The other parameters have the following value

$$\begin{aligned} a_0 = 6.75, \quad a_1 = -1.95, \quad a_2 = 2.625, \\ a_3 = -7.44, \quad b_3 = 0.75, \quad b_4 = 7.5. \end{aligned}$$

The other choice of effective potential was proposed in Ref. [19] and has the logarithmic form. The result produced by this potential are known to be fitted well to lattice results.

$$\begin{aligned} \frac{\mathcal{U}_{\text{log}}(\Phi, \Phi^*, T)}{T^4} = & -\frac{a(T)}{2} \Phi^* \Phi + b(T) \ln[1 - 6\Phi^* \Phi \\ & + 4(\Phi^{*3} + \Phi^3) - 3(\Phi^* \Phi)^2] \end{aligned} \quad (9)$$

TABLE I: The squared masses of scalar and pseudoscalar meson appear in nonstrange strange basis. In the following table x denotes σ_x and y denotes σ_y . The masses of nonstrange σ_{NS} , strange σ_S , nonstrange η_{NS} and strange η_S mesons is in last two rows.

Scalar Meson Sector		Pseudoscalar Meson Sector	
$m_{a_0}^2$	$m^2 + \lambda_1(x^2 + y^2) + \frac{3\lambda_2}{2}x^2 + \frac{\sqrt{2}c}{2}y$	m_π^2	$m^2 + \lambda_1(x^2 + y^2) + \frac{\lambda_2}{2}x^2 - \frac{\sqrt{2}c}{2}y$
m_κ^2	$m^2 + \lambda_1(x^2 + y^2) + \frac{\lambda_2}{2}(x^2 + \sqrt{2}xy + 2y^2) + \frac{c}{2}x$	m_K^2	$m^2 + \lambda_1(x^2 + y^2) + \frac{\lambda_2}{2}(x^2 - \sqrt{2}xy + 2y^2) - \frac{c}{2}x$
$m_{s,00}^2$	$m^2 + \frac{\lambda_1}{3}(7x^2 + 4\sqrt{2}xy + 5y^2) + \lambda_2(x^2 + y^2) - \frac{\sqrt{2}c}{3}(\sqrt{2}x + y)$	$m_{p,00}^2$	$m^2 + \lambda_1(x^2 + y^2) + \frac{\lambda_2}{3}(x^2 + y^2) + \frac{c}{3}(2x + \sqrt{2}y)$
$m_{s,88}^2$	$m^2 + \frac{\lambda_1}{3}(5x^2 - 4\sqrt{2}xy + 7y^2) + \lambda_2(\frac{x^2}{2} + 2y^2) + \frac{\sqrt{2}c}{3}(\sqrt{2}x - \frac{y}{2})$	$m_{p,88}^2$	$m^2 + \lambda_1(x^2 + y^2) + \frac{\lambda_2}{6}(x^2 + 4y^2) - \frac{c}{6}(4x - \sqrt{2}y)$
$m_{s,08}^2$	$\frac{2\lambda_1}{3}(\sqrt{2}x^2 - xy - \sqrt{2}y^2) + \sqrt{2}\lambda_2(\frac{x^2}{2} - y^2) + \frac{c}{3\sqrt{2}}(x - \sqrt{2}y)$	$m_{p,08}^2$	$\frac{\sqrt{2}\lambda_2}{6}(x^2 - 2y^2) - \frac{c}{6}(\sqrt{2}x - 2y)$
m_σ^2	$m_{s,00}^2 \cos^2 \theta_s + m_{s,88}^2 \sin^2 \theta_s + 2m_{s,08}^2 \sin \theta_s \cos \theta_s$	$m_{\eta'}^2$	$m_{p,00}^2 \cos^2 \theta_p + m_{p,88}^2 \sin^2 \theta_p + 2m_{p,08}^2 \sin \theta_p \cos \theta_p$
$m_{f_0}^2$	$m_{s,00}^2 \sin^2 \theta_s + m_{s,88}^2 \cos^2 \theta_s - 2m_{s,08}^2 \sin \theta_s \cos \theta_s$	m_η^2	$m_{p,00}^2 \sin^2 \theta_p + m_{p,88}^2 \cos^2 \theta_p - 2m_{p,08}^2 \sin \theta_p \cos \theta_p$
$m_{\sigma_{NS}}^2$	$\frac{1}{3}(2m_{s,00}^2 + m_{s,88}^2 + 2\sqrt{2}m_{s,08}^2)$	$m_{\eta_{NS}}^2$	$\frac{1}{3}(2m_{p,00}^2 + m_{p,88}^2 + 2\sqrt{2}m_{p,08}^2)$
$m_{\sigma_S}^2$	$\frac{1}{3}(m_{s,00}^2 + 2m_{s,88}^2 - 2\sqrt{2}m_{s,08}^2)$	$m_{\eta_S}^2$	$\frac{1}{3}(m_{p,00}^2 + 2m_{p,88}^2 - 2\sqrt{2}m_{p,08}^2)$

where the temperature dependent coefficients are as follow

$$a(T) = a_0 + a_1 \left(\frac{T_0}{T}\right) + a_2 \left(\frac{T_0}{T}\right)^2 \quad b(T) = b_3 \left(\frac{T_0}{T}\right)^3.$$

The critical temperature for deconfinement phase transition $T_0 = 270$ MeV is fixed for pure gauge sector. The parameters of eq.(9) are

$$\begin{aligned} a_0 &= 3.51, & a_1 &= -2.47, \\ a_2 &= 15.2, & b_3 &= -1.75 \end{aligned}$$

Both fits reproduce equally well the equation of state and the Polyakov loop expectation value.

III. GRAND POTENTIAL IN THE MEAN FIELD APPROACH

The thermodynamics of changing numbers of particles and antiparticles is governed by grand canonical partition function. We are considering a spatially uniform system in thermal equilibrium at finite temperature T and quark chemical $\mu_f (f = u, d, s)$. The partition function is written as the path integral over quark/antiquark and meson fields [41]

$$\begin{aligned} \mathcal{Z} &= \text{Tr} \exp[-\beta(\hat{\mathcal{H}} - \sum_{f=u,d,s} \mu_f \hat{N}_f)] \\ &= \int \prod_a \mathcal{D}\sigma_a \mathcal{D}\pi_a \int \mathcal{D}q \mathcal{D}\bar{q} \\ &\quad \exp \left[- \int_0^\beta d\tau \int_V d^3x \left(\mathcal{L}_{QMS} + \sum_{f=u,d,s} \mu_f \bar{q}_f \gamma^0 q_f \right) \right] \end{aligned} \quad (10)$$

where V is the three dimensional volume of the system, and $\beta = \frac{1}{T}$. For three quark flavors, in general, the three quark chemical potential are different. In this work, we assume that $SU_V(2)$ symmetry is preserved and neglect

the small difference in masses of u and d quarks. Thus the quark chemical potential for u and d quarks become equal $\mu_x = \mu_u = \mu_d$. The strange quark chemical potential is μ_s . Further we consider symmetric quark matter and net baryon number is zero.

In the following, we adopt meanfield approximation to perform our calculation of partion function [35, 40, 41]. We replace meson field by their expectation values $\langle \Phi \rangle = T_0 \bar{\sigma}_0 + T_8 \bar{\sigma}_8$ and neglect both thermal as well as quantum fluctuations of meson fields while quarks and antiquarks are retained as quantum field. Now following the standard procedure as given in Refs. [16, 18, 43, 44] one can obtain the expression of grand potential as sum of pure gauge field contribution $\mathcal{U}(\Phi, \Phi^*, T)$, meson contribution and quark/antiquark contribution evaluated in the presence of Polyakov loop,

$$\Omega(T, \mu) = -\frac{T \ln Z}{V} = U(\sigma_0, \sigma_8) + \mathcal{U}(\Phi, \Phi^*, T) + \Omega_{\bar{q}q}(T, \mu) \quad (11)$$

In order to study $2 + 1$ flavor case, one performs following basis transformation of condensates and external fields from original singlet octet $(0, 8)$ basis to nonstarange strange basis (x, y) .

$$\sigma_x = \sqrt{\frac{2}{3}} \bar{\sigma}_0 + \frac{1}{\sqrt{3}} \bar{\sigma}_8, \quad (12)$$

$$\sigma_y = \frac{1}{\sqrt{3}} \bar{\sigma}_0 - \sqrt{\frac{2}{3}} \bar{\sigma}_8. \quad (13)$$

Similar expressions exist for writing the external fields (h_x, h_y) in terms of (h_0, h_8) . Thus the nonstarange and strange quark/antiquark dcouple and the meson masses becomes

$$m_x = g \frac{\sigma_x}{2}, \quad m_y = g \frac{\sigma_y}{\sqrt{2}} \quad (14)$$

Quarks become massive in symmetry breaking phase because of non zero vacuum expectation values of condensates.

TABLE II: parameters for $m_\sigma = 600$ MeV with and without $U_A(1)$ axial term.

	C[MeV]	m^2 [MeV ²]	λ_1	λ_2	h_x [MeV ³]	h_y [MeV ³]
W/ $U_A(1)$	4807.84	342.52	1.40	46.48	(120.73) ³	(336.41) ³
W/o $U_A(1)$	0	-(189.85) ²	-17.01	82.47	(120.73) ³	(336.41) ³

The mesonic potential in the nonstrange-strange basis reads,

$$\begin{aligned}
U(\sigma_x, \sigma_y) = & \frac{m^2}{2} (\sigma_x^2 + \sigma_y^2) - h_x \sigma_x - h_y \sigma_y - \frac{c}{2\sqrt{2}} \sigma_x^2 \sigma_y \\
& + \frac{\lambda_1}{2} \sigma_x^2 \sigma_y^2 + \frac{1}{8} (2\lambda_1 + \lambda_2) \sigma_x^4 \\
& + \frac{1}{8} (2\lambda_1 + 2\lambda_2) \sigma_y^4, \quad (15)
\end{aligned}$$

The chiral part of PQM model has the six input parameters and therefore require six known quantities as input. In general m_π , m_K , the pion and kaon decay constant f_π , f_K , mass square of η , η' and m_σ are used to fix these parameters. The parameters are fitted such that in vacuum the model produces observed pion mass 138 MeV. In the present work we are the set of parameters for sigma mass $m_\sigma = 600$ MeV. The parameters used in this work, taken from [41], are shown in Table II.

Finally the quark/antiquark Polyakov loop contribution reads,

$$\Omega_{\bar{q}q}(T, \mu) = -2T \sum_{f=u,d,s} \int \frac{d^3p}{(2\pi)^3} [\ln g_f^+ + \ln g_f^-] \quad (16)$$

We define g_f^+ and g_f^- after taking trace over color space

$$g_f^+ = \left[1 + 3\Phi e^{-E_f^+/T} + 3\Phi^* e^{-2E_f^+/T} + e^{-3E_f^+/T} \right] \quad (17)$$

$$g_f^- = \left[1 + 3\Phi^* e^{-E_f^-/T} + 3\Phi e^{-2E_f^-/T} + e^{-3E_f^-/T} \right] \quad (18)$$

Here we use the notation $E_f^\pm = E_f \mp \mu$ and E_f is the flavor dependent single particle energy of quark/antiquark.

$$E_f = \sqrt{p^2 + m_f^2} \quad (19)$$

m_f is flavor dependent quark masses and is function of condensates σ_0 and σ_8 .

One can very easily notice from equations (17) and (18) that the role of quarks and antiquarks as well as that of Polyakov loop and its conjugate can be interchanged by the transformation $\mu \rightarrow -\mu$. Confinement is the very interesting feature of the QCD and the PQMS model describes this behaviour qualitatively. Polyakov loop is order parameter for confinement deconfinement phase transition. In the confined phase $\Phi = 0$. It can also be noticed from the grand potential that one and two quarks state contributions are vanish. Only the three quark

states contribute. In this way PQMS model qualitatively mimics confinement of quark/antiquark within three quark color singlet states [22].

One can get the quark condensates σ_x , σ_y and Polyakov loop expectation values Φ , Φ^* by searching the global minima of the grand potential for a given value of temperature T and chemical potential μ .

$$\left. \frac{\partial \Omega}{\partial \sigma_x} = \frac{\partial \Omega}{\partial \sigma_y} = \frac{\partial \Omega}{\partial \Phi} = \frac{\partial \Omega}{\partial \Phi^*} \right|_{\sigma_x = \bar{\sigma}_x, \sigma_y = \bar{\sigma}_y, \Phi = \bar{\Phi}, \Phi^* = \bar{\Phi}^*} = 0. \quad (20)$$

In this work we are always considering the $\mu = 0$ case.

IV. MESON MASSES AND MIXING ANGLES

The curvature of grand potential eq (11) at the global minimum determines scalar and pseudoscalar meson masses.

$$m_{\alpha,ab}^2 = \left. \frac{\partial^2 \Omega(T, \mu)}{\partial \xi_{\alpha,a} \partial \xi_{\alpha,b}} \right|_{min} \quad (21)$$

where subscript $\alpha = s, p$, where s stands for scalar and p stands for pseudoscalar meson and $a, b = 0 \dots 8$. We note that the Polyakov loop decouples from the mesonic sector at $T=0$ and the meson masses do not receive contribution from quark/antiquark in vacuum and hence meson masses are governed by mesonic potential only. The mesonic contribution to the meson masses is summarized

	$m_{i,a}^2 m_{f,b}^2 / g^4$	$m_{i,ab}^2 / g^2$	$m_{s,a}^2 m_{f,b}^2 / g^4$	$m_{s,ab}^2 / g^2$
$\sigma_0 \sigma_0$	$\frac{1}{3} \sigma_x^2$	$\frac{2}{3}$	$\frac{1}{3} \sigma_y^2$	$\frac{1}{3}$
$\sigma_1 \sigma_1$	$\frac{1}{2} \sigma_x^2$	1	0	0
$\sigma_4 \sigma_4$	0	$\sigma_x \frac{\sigma_x + \sqrt{2} \sigma_y}{\sigma_x^2 - 2\sigma_y^2}$	0	$\sigma_y \frac{\sqrt{2} \sigma_x + 2\sigma_y}{2\sigma_y^2 - \sigma_x^2}$
$\sigma_8 \sigma_8$	$\frac{1}{6} \sigma_x^2$	$\frac{1}{3}$	$\frac{2}{3} \sigma_y^2$	$\frac{2}{3}$
$\sigma_0 \sigma_8$	$\frac{\sqrt{2}}{6} \sigma_x^2$	$\frac{\sqrt{2}}{3}$	$-\frac{\sqrt{2}}{3} \sigma_y^2$	$-\frac{\sqrt{2}}{3}$
$\pi_0 \pi_0$	0	$\frac{2}{3}$	0	$\frac{1}{3}$
$\pi_1 \pi_1$	0	1	0	0
$\pi_4 \pi_4$	0	$\sigma_x \frac{\sigma_x - \sqrt{2} \sigma_y}{\sigma_x^2 - 2\sigma_y^2}$	0	$\sigma_y \frac{\sqrt{2} \sigma_x - 2\sigma_y}{\sigma_x^2 - 2\sigma_y^2}$
$\pi_8 \pi_8$	0	$\frac{1}{3}$	0	$\frac{2}{3}$
$\pi_0 \pi_8$	0	$\frac{\sqrt{2}}{3}$	0	$-\frac{\sqrt{2}}{3}$

TABLE III: First and second derivative of squared quark mass in nonstrange-strange basis with respect to meson fields are evaluated at minimum. Sum over two light flavors, denoted by symbol l , is in third and fourth column. The last two columns have only strange quark mass flavor denoted by symbol s .

in Table I. The diagonalization of (0 - 8) component of mass matrix gives masses of σ and f_0 mesons in scalar sector and masses of η' and η in pseudoscalar sector. The scalar mixing angle θ_s and pseudoscalar mixing angle θ_p .

$$\tan 2\theta_\alpha = \left(\frac{2m_{\alpha,08}^2}{m_{\alpha,00}^2 - m_{\alpha,88}^2} \right) \quad (22)$$

Here α stands for scalar and pseudoscalar field. The detail expressions for masses and mixing angles are given [37, 41]. The meson masses are further modified in medium at finite temperature by the quark contributions in the grand potential. In order to calculate the second derivative $\partial^2 \Omega / \partial \xi_{\alpha,a}^2$ for evaluating the quark contribution in the presence of Polyakov loop potential, the complete dependence of all scalar and pseudoscalar meson fields (Eq.6) has to be taken into account. We have to diagonalize the resulting quark mass matrix. The expression for the meson mass modification due to quark contribution at finite temperature in QMS model, has been evaluated by Schaefer et al. [41].

The expression of mass modification due to quark contribution at finite temperature, will change in the presence of Polyakov loop. We are obtaining the following formula for the mass modification that results on account of quark contribution in the PQMS model

$$\begin{aligned} \delta m_{\alpha,ab}^2 &= \frac{\partial^2 \Omega_{\bar{q}q}(T, \mu)}{\partial \xi_{\alpha,a} \partial \xi_{\alpha,b}} \Big|_{min} = 3 \sum_{f=x,y} \int \frac{d^3p}{(2\pi)^3} \frac{1}{E_f} \\ &\left[(A_f^+ + A_f^-) \left(m_{f,ab}^2 - \frac{m_{f,a}^2 m_{f,b}^2}{2E_f^2} \right) \right. \\ &\left. + (B_f^+ + B_f^-) \left(\frac{m_{f,a}^2 m_{f,b}^2}{2E_f T} \right) \right] \quad (23) \end{aligned}$$

$m_{f,a}^2 \equiv \partial m_f^2 / \partial \xi_{\alpha,a}$ is first the derivative and $m_{f,ab}^2 \equiv \partial^2 m_f^2 / \partial \xi_{\alpha,a} \partial \xi_{\alpha,b}$ is the second derivative of squared quark mass with respect to meson fields $\xi_{\alpha,a}$.

The notations A_f^\pm and B_f^\pm have the following definitions

$$A_f^+ = \frac{\Phi e^{-E_f^+/T} + 2\Phi^* e^{-2E_f^+/T} + e^{-3E_f^+/T}}{g_f^+} \quad (24)$$

$$A_f^- = \frac{\Phi^* e^{-E_f^-/T} + 2\Phi e^{-2E_f^-/T} + e^{-3E_f^-/T}}{g_f^-} \quad (25)$$

and $B_f^\pm = 3(A_f^\pm)^2 - C_f^\pm$ where we again define

$$C_f^+ = \frac{\Phi e^{-E_f^+/T} + 4\Phi^* e^{-2E_f^+/T} + 3e^{-3E_f^+/T}}{g_f^+} \quad (26)$$

$$C_f^- = \frac{\Phi^* e^{-E_f^-/T} + 4\Phi e^{-2E_f^-/T} + 3e^{-3E_f^-/T}}{g_f^-} \quad (27)$$

The squared quark mass derivatives evaluated at minimum, that were originally derived in Ref.[41], are collected in Table III. The inclusion of Polyakov loop in QMS model does not make any change in these equations.

V. EFFECT OF POLYAKOV LOOP ON RESTORATION OF CHIRAL SYMMETRY

We are presenting the result of our calculation for estimating the effect of Polyakov loop potential on the restoration of chiral symmetry when it is included in the 2 + 1 flavor linear sigma model at finite temperature and

	QMS	PQMSM log	PQMSM pol
T_c^x (MeV)	146	206	204
T_s^x (MeV)	270	274	262
T_c^Φ (MeV)	—	206	204

TABLE IV: The characteristic temperature (pseudocritical temperature) for the chiral transition in the nonstrange sector T_c^x , strange sector T_s^x and confinement-deconfinement transition T_c^Φ , in QMS, PQMS:log and in PQMS:pol model.

zero chemical potential with and without axial $U_A(1)$ breaking. We have considered the two different ansatzs for Polyakov loop potential namely the polynomial potential and logarithmic potential and compared the results with the existing calculations in the Quark Meson Linear Sigma Model[41]. The interplay of the effect of $U_A(1)$ axial restoration and chiral symmetry restoration in the presence of Polyakov loop potential has been shown through the temperature variation of strange, non-strange chiral condensates, meson masses and mixing angles. The $U_A(1)$ axial breaking term has been kept constant throughout the investigation. The value of Yukawa coupling g has been fixed from the nonstrange constituent quark mass $m_q = 300$ MeV and is equal to 6.5. This predicts the strange quark mass $m_s \simeq 433$ MeV.

A. Condensates and the Polyakov Loop

The temperature dependence of the Polyakov loop expectation value $\langle \Phi \rangle$, nonstrange and strange condensates at zero chemical potential, is obtained from the solution of the gap equations (20) and the inflection points of these order parameters respectively give the characteristic temperature (pseudocritical temperature) for the confinement-deconfinement transition T_c^Φ , the chiral transition in the nonstrange T_c^x and strange sector T_s^x . The numerical value of the pseudocritical temperature for various transitions in Quark Meson Sigma (QMS) model and Polyakov loop Quark Meson Sigma Model (PQMS) with polynomial (Eq.8) and logarithmic (Eq.9) potentials for the Polyakov loop has been given in Table IV. It is evident from the table

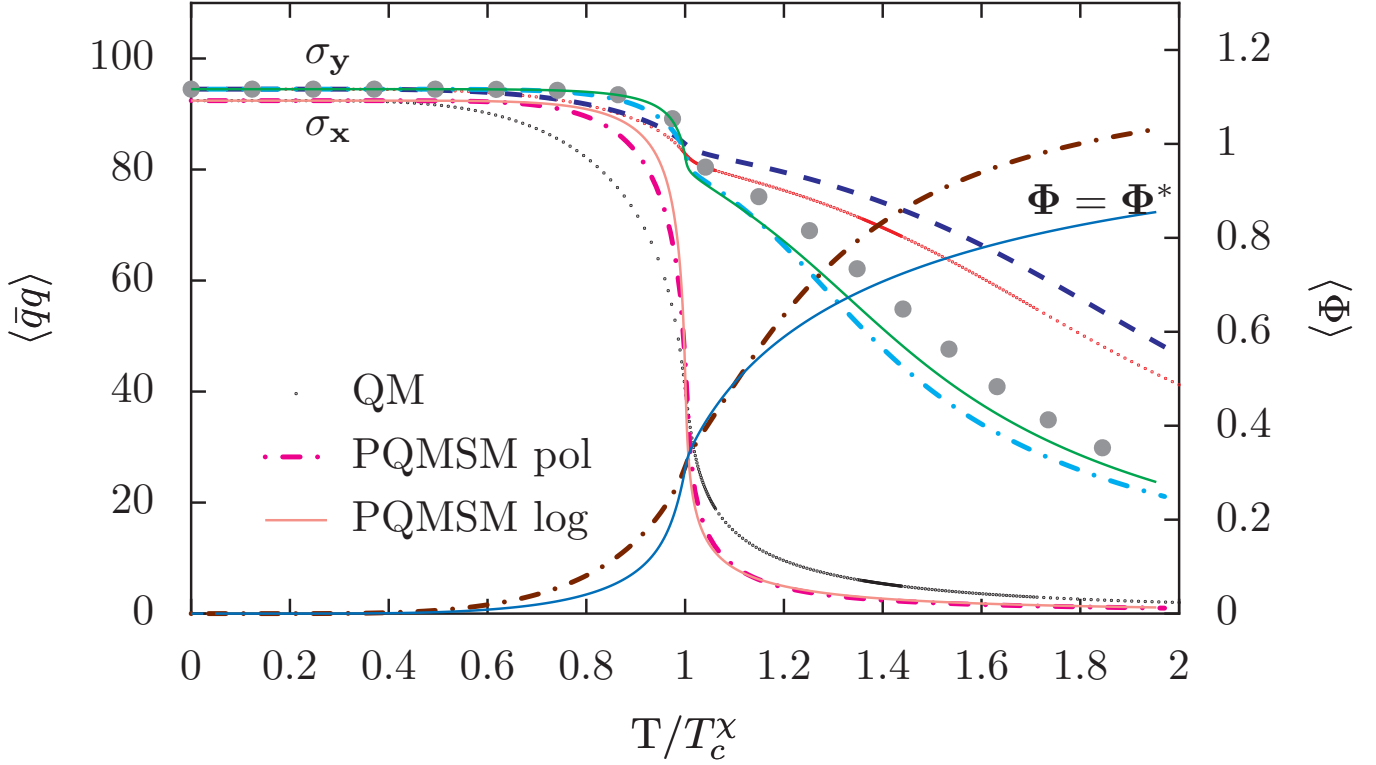


FIG. 1: shows the variation of nonstrange σ_x , strange σ_y condensates with respect to the relative temperature scale at zero chemical potential in the QMS model and PQMS models with polynomial and logarithmic potentials for the Polyakov loop. The lines with continuous dots represent the variation in QMS model while the dash dot lines show the variation in PQMS pol model and the solid lines are the variations in PQMS log model. The line with big solid dots shows the σ_y variation in the PQMS:log model while the dark dash line shows the pure QMS model results when anomaly is absent i.e. $c = 0$.

that the chiral transition gets shifted to the higher temperatures as a result of the inclusion of Polyakov loop in the QMS model. Further it is reported in Ref [15] that for the most of the parameter sets $T_c^x > T_c^\Phi$. Such a behaviour is on the expected lines because the fermionic contributions to the thermodynamic potential are suppressed due to the influence of the Polyakov loop and since the chiral phase transition is driven by fermionic contributions, chiral restoration gets delayed on account of the ensuing delay in the deconfinement transition. Here it is pertinent to mention that larger values of m_σ and T_0 also shifts the chiral and deconfinement transition temperatures to higher values [15]. The value of the parameters m_σ and T_0 has been taken as 600 MeV and 270 MeV respectively in our calculation because using different versions of Polyakov loop potential, one gets coincident chiral and deconfinement transitions with these parameter sets [15].

We have chosen to compare the results of our calculation in the PQMS model with the corresponding results in the QMS model on a relative temperature scale T/T_c^x . Such a choice is justified on account of the Ginsburg-Landau effective theory, where absolute comparison of the characteristic temperatures between two models of the same universality class can not be

made[31]. Further since the focus of our investigation is the influence of Polyakov loop on effective restoration of symmetries, we will be comparing the mesonic observables below and above T_c^x . Fig.1 shows the variation of nonstrange σ_x , strange σ_y condensates with respect to the relative temperature scale at zero chemical potential in the QMS model and PQMS models with polynomial (Eq.8) and logarithmic (Eq.9) potentials for the Polyakov loop. The lines with continuous dots represent the variation in QMS model while the dash dot lines show the variation in PQMS pol model and the solid lines are the variations in PQMS log model. The condensates start with fixed values $\sigma_x = 92.4$ MeV and $\sigma_y = 94.5$ MeV at $T = 0$. The presence of $U_A(1)$ anomaly does not cause any difference in the behaviour of the nonstrange condensate whose variation in the $T/T_c^x = 0.7$ to 1.5 range becomes sharp in the Polyakov loop augmented QMS models when it is compared with the pure QMS model result. The logarithmic potential for the Polyakov loop produces the sharpest chiral crossover transition in the nonstrange sector. The variation of the strange condensate is lot more smooth on account of the large constituent mass of the strange quark $m_s = 433$ MeV. The dotted line (QMS model), dash dotted line (PQMS:pol model) and solid line (PQMS:log model)

variations for the strange condensate σ_y , have been calculated in the presence of explicit $U(1)_A$ symmetry breaking term (constant 'tHooft coupling $c = 4807.84$ MeV). For comparison, the σ_y behaviour has also been calculated in the absence of $U(1)_A$ symmetry breaking ($c = 0$) term. The line with big solid dots shows the σ_y variation in the logarithmic Polyakov loop potential augmented QMS model while the dark dash line shows the pure QMS model results when $c = 0$.

The Presence of axial anomaly in the pure QMS model causes a little earlier melting [41] of the strange condensate while in comparison, the presence of Polyakov loop potential in QMS model generates a significant melting of the strange condensate. We infer from the solid PQMS:log and dash dot PQMS:pol curves in PQMS models that the inclusion of Polyakov loop in QMS model together with the presence of axial anomaly, triggers quite an early melting of the strange condensate. The earlier melting of the strange condensate in PQMS models in comparison to the pure QMS model result, indicates an early set up of the $U(1)_A$ restoration trend on the relative temperature scale in the PQMS models. Curves starting from the right end of the plot represent the variation of the Polyakov loop expectation value Φ on the relative temperature scale at zero chemical potential, here also the solid line corresponds to the variation in PQMS:log model and the dash dot line shows the variation in the PQMS:pol model. Here, we would like to mention that the expectation value $\langle \Phi \rangle$ increases above unity and hence its interpretation as an order parameter, related to the free energy of a static color charge, gets compromised [15]. However, these findings are in consonance with other model investigations for three quark flavour/cite Ming chinese. The logarithmic divergence avoids expectation value higher than one for the other Polyakov loop potential.

B. Meson Mass Variations

We are calculating the masses of the scalar and pseudoscalar mesons in medium at finite temperature. The vacuum values of these masses have been evaluated in [37, 41]. We have collected the vacuum value of all the masses and mixing angles in Table I. The mass modifications, obtained in PQMS model (Eq.23), in the finite temperature medium, will be added to the vacuum masses of Table I. For finite temperature mass modifications in QMS model, we are using the formula B12 of Ref.[41]. We will be discussing the mass variations of the scalar and pseudoscalar meson nonets with respect to the reduced temperature T/T_c^x scale at zero chemical potential. The mass variations of the chiral partners as functions of reduced temperature, in the presence of axial $U_A(1)$ breaking term, are plotted for (σ, π) and (a_0, η') in Fig.2(a) and for (η, f_0) and (K, κ) in Fig.3(a), while the corresponding mass variations, in the absence of the $U_A(1)$ axial breaking term, are plotted in Fig.2(b) and

Fig.3(b). As per our choice of symbols, the dotted line plots are the mass variations in the pure QMS model, dash dot line plots represent the PQMS:pol model results and the solid line plots are the mass variations in the PQMS:log model.

The chiral partners (σ, π) and (a_0, η') become degenerate in mass in Fig.2(a) in the close vicinity of reduced temperature $T/T_c^x = 1$. We notice that the mass degeneration is a little diffused in pure QMS model while in the Polyakov augmented PQMS models, this mass degeneration occurs almost exactly at $T/T_c^x = 1$. Further the sharpest variation in the masses is noticed for the PQMS:log model while the PQMS:pol model results, also show sharper variation in comparison to the pure QMS model mass variations. This sharpening of the mass variations in the small neighbourhood of $T/T_c^x = 1$ results due to the stronger and sharper melting of the nonstrange condensate (as shown in Fig.1) triggered by the presence of Polyakov loop potential in the QMS model. Thus we can corroborate, also from the behaviour of the chiral partners that the net effect of the Polyakov loop inclusion in the QMS model, is to make a sharper occurrence of chiral $SU_L(2) \times SU_R(2)$ symmetry restoration transition in the nonstrange sector (almost exactly at the reduced temperature $T/T_c^x = 1$) which is a smooth crossover in pure QMS model. In Fig.3(a), the presence of Polyakov loop potential in the two PQMS models (namely PQMS:log and PQMS:pol) generates, the similar trend of sharpening in mass variations for the chiral partners (η, f_0) and (K, κ) . Though the mass degeneration of chiral partners (K, κ) with η does not occur when the value of the reduced temperature is equal to one, it sets up early in the two PQMS models at $T/T_c^x = 1.3$ while it occurs at $T/T_c^x = 1.5$ in the pure QMS model. In the two PQMS models, the intersection point of the f_0 and η masses, occurs early when the reduced temperature $T/T_c^x = 1.4$ while in pure QMS model this intersection point is found at $T/T_c^x = 1.7$. This trend of mass degeneration emerges, again as a result of the sharper and stronger melting of the strange condensate (Fig.1) in the influence of the Polyakov loop potential in the PQMS models.

The $U_A(1)$ breaking generates the mass gap between the two sets of the chiral partners (σ, π) and (a_0, η') i.e. $m_\pi = m_\sigma < m_{a_0} = m_{\eta'}$ for $T/T_c^x > 1$. This mass gap results due to the opposite sign of the anomaly term in the scalar and pseudoscalar meson masses[41]. The anomaly term is $\sqrt{2}c\sigma_y$. The nonstrange condensate σ_x becomes negligible for $T/T_c^x > 1$. The above mentioned mass gap will be reduced due to the melting of the strange order parameter σ_y for higher value of the reduced temperature $T/T_c^x > 1$. Since the melting of the strange condensate is stronger and sharper (as shown in Fig.1) in the Polyakov loop augmented PQMS models, the convergence in the masses of the two sets of chiral partners will be enhanced in these models. Hence the inclusion of Polyakov loop potential in the PQMS models also effects an early set up of $U_A(1)$ restoration trend

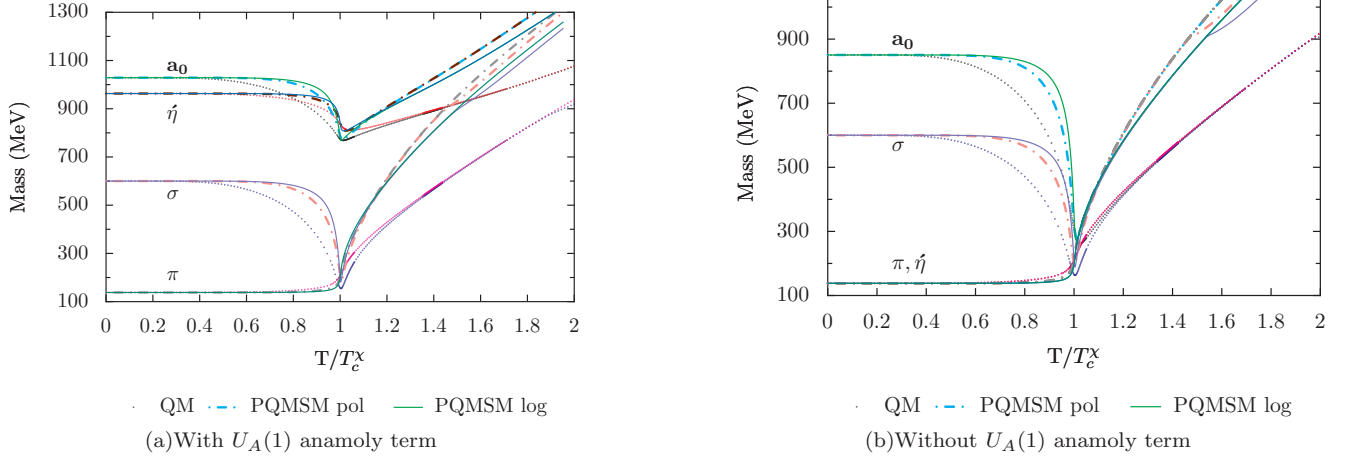


FIG. 2: The mass variations of the chiral partners as functions of reduced temperature, in the presence of axial $U_A(1)$ breaking term, are plotted for (σ, π) and (a_0, η') in Fig.2(a) while the corresponding mass variations, in the absence of the $U_A(1)$ axial breaking term, are plotted in Fig.2(b). As per our choice of symbols, the dotted line plots are the mass variations in the pure QMS model, dash dot line plots represent the PQMS:pol model results and the solid line plots are the mass variations in the PQMS:log model.

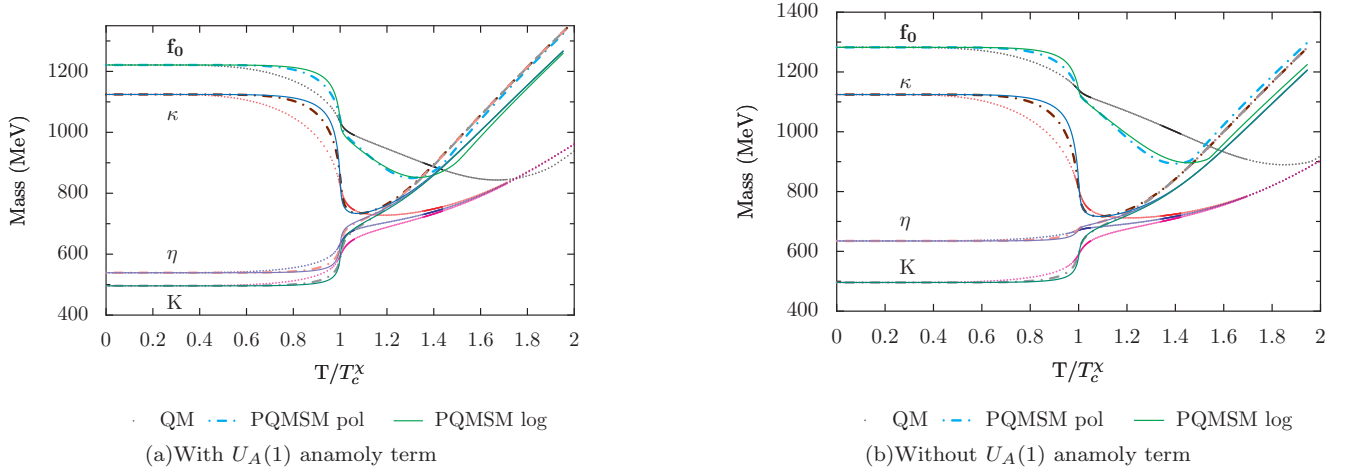


FIG. 3: The mass variations of the chiral partners as functions of reduced temperature, in the presence of axial $U_A(1)$ breaking term, are plotted for (η, f_0) and (K, κ) in Fig.3(a), while the corresponding mass variations, in the absence of the $U_A(1)$ axial breaking term, are plotted in Fig.3(b). As per our choice of symbols, the dotted line plots are the mass variations in the pure QMS model, dash dot line plots represent the PQMS:pol model results and the solid line plots are the mass variations in the PQMS:log model.

on the reduced temperature scale. Thus the $U_A(1)$ restoration in PQMS models will finally occur at smaller value of the reduced temperature when a comparison is made with QMS model result.

Now we discuss the variations in the masses of chiral partners when the explicit $U(1)_A$ symmetry breaking term has been taken as zero ($c = 0$). We notice in Fig.2(b) and Fig.3(b), again the same sharpening trend of mass variations that we identify as the effect generated by the inclusion of Polyakov loop potential. The η' meson degenerates with the pion in vacuum and stays the same for all temperatures in Fig.2(b) due to the absence of the

anomaly term. Further the mass gap between the chiral partners (σ, π) and (a_0, η') becomes zero and all the four mesons become degenerate at $T/T_c^X = 1$. The mass degeneration in the close vicinity of T_c^X is a little diffused in the QMS model. It becomes sharp in the two PQMS models and occurs almost exactly at $T/T_c^X = 1$.

Though the spontaneously broken axial $U_A(1)$ gets restored for $T \geq T_c^X$, the full restoration of $U(3) \times U(3)$ symmetry is yet not complete because the mass degeneration of chiral partners (K, κ) with the η in Fig.3(b) does not take place when the reduced temperature $T/T_c^X = 1$ and it sets up early in the

two PQMS models at $T/T_c^x = 1.3$ while it occurs at $T/T_c^x = 1.5$ in the pure QMS model. Here, it is pertinent to emphasize that the T/T_c^x numerical value, where the K , κ and η masses degenerate in different models, is not influenced by the $U_A(1)$ anomaly as expected since the nonstrange condensate does not have any anomaly dependence. Though the Ref [32] in a mean field NJL model study, finds a clear difference for the nonstrange chiral transition in the presence and absence of the explicit $U_A(1)$ breaking anomaly term. Further, in Fig.3(b), the intersection point of the f_0 and η masses in the two PQMS models, is obtained when the reduced temperature T/T_c^x is around 1.6 while in the pure QMS model, this intersection point is found around $T/T_c^x = 2.0$. We are also obtaining the mild anomaly dependence of the intersection point of the f_0 and η in all the models as pointed out in ref [41] for pure QMS model. Here, we also remind that the mass of f_0 in vacuum increases by about 60 MeV in the absence of anomaly.

The last important thing of this section is the observation and location of the kink in the mass variation of scalar σ and f_0 on the reduced temperature scale. This kink occurs around $T/T_c^x = 1.8$ in the QMS model while it is seen around $T/T_c^x = 1.4$ in PQMS models. The kink generation results because the meson masses seem to interchange their identities for higher values of the reduced temperature [41]. In order to have a proper perspective of the kink behaviour in the curves, one has to study and analyze the scalar and pseudoscalar meson mixing angles.

C. Meson Mixing Angle Variations

The definitions and expressions for the mixing angles in different bases and formulae for their calculations are given in Ref.[41]. We have collected these formulae in Table I. We are using this data set for all the calculations presented in this subsection. The identification of axial $U_A(1)$ restoration pattern will become complete, only after studying the variation of isoscalar, scalar and pseudoscalar mixing angles on the relative temperature scale. The scalar θ_s and pseudoscalar θ_p mixing angle variations with respect to the reduced temperature at zero chemical potential are plotted in Fig.4. We have given the plots for QMS, PQMS:log and PQMS:pol models considering the cases in the presence as well as absence of axial $U_A(1)$ explicit symmetry breaking term. The dotted lines show the result with anomaly in QMS model while the solid big dot lines show the result without anomaly. In PQMS:log model, thick solid lines represent the variations without anomaly while thin solid lines show the result with anomaly. Dash dotted lines are the variations with anomaly in PQMS:pol model, while dash lines are the corresponding results in the absence of anomaly. Same as the findings of Ref.[41], the anomaly term has a strong effect in the pseudoscalar sector in the

broken phase for $T/T_c^x < 1$ while no effect of anomaly is found in the scalar sector, here, in all the model calculations. The nonstrange and strange quark mixing is strong, at $T = 0$ one gets $\theta_p = -5^\circ$ which remains almost constant in the chiral broken phase. In the vicinity of $T/T_c^x = 1$, the θ_p variations start approaching the ideal mixing angle θ_p tends to $\arctan(\frac{1}{\sqrt{2}}) \approx 35^\circ$, the corresponding $\phi_p = 90^\circ$. Here ϕ_p is the pseudoscalar mixing angle in the strange nonstrange basis (see Ref.[41] for details). The smooth approach towards the ideal mixing in QMS model, becomes sharp in the two PQMS models due to the influence of Polyakov loop potential. Further, in comparison to QMS model results, the ideal mixing on the reduced temperature scale is achieved a little earlier in the PQMS models. In the absence of axial $U_A(1)$ anomaly, the pseudoscalar mixing angle remains ideal $\theta_p = 35^\circ$ everywhere on the reduced temperature scale, in all the presented model calculations. This means that η' is a purely light quark system and the η is a pure strange quark system. Thus either in the presence or in the absence of anomaly term the η' meson will act as a chiral partner of pion.

The η and η' mesons become a purely strange η_S and nonstrange η_{NS} quark system as a consequence of the ideal pseudoscalar mixing which gets fully achieved in the pseudoscalar sector at higher values of the reduced temperature. In order to show this, we have plotted in Fig.5(a) the mass variations for the physical η , η' and the nonstrange-strange η_{NS} , η_S complex, on the reduced temperature scale. Mass formulae $m_{\eta_{NS}}$ and m_{η_S} are given in table I. Again the smooth mass convergence trend, of pure QMS model in $m_{\eta'} \rightarrow m_{\eta_{NS}}$ and $m_\eta \rightarrow m_{\eta_S}$ approach, becomes sharp around $T/T_c^x = 1$ in the Polyakov loop augmented QMS models. The exact $\eta' \rightarrow \eta_{NS}$ and $\eta \rightarrow \eta_S$ mass convergence in PQMS models, occurs at a value which is a bit closer to $T/T_c^x = 1$ when a comparison is made with the corresponding value obtained in the QMS model.

It is evident from Fig.4 that the mixing angle in the scalar sector θ_s is not affected by the axial anomaly in the broken phase. The precise vacuum value of θ_s depends on the chosen value of the sigma meson mass m_σ while the pseudoscalar mixing angle shows no sigma mass dependence. For $m_\sigma = 600 \text{ MeV}$, a value chosen for our present calculations $\theta_s \sim 19.9^\circ$ at $T=0$. For increasing m_σ scalar mixing angle θ_s also increases [41]. The θ_s around $T/T_c^x = 1$ grows to its ideal value but for higher temperatures on the reduced temperature scale, in the chirally symmetric phase, the scalar mixing angle drops down to $\theta_s \sim -51^\circ$. In the presence of $U_A(1)$ symmetry breaking term, this drop happens in the QMS model for $T/T_c^x \sim 1.85$ and in the PQMS:log model, the similar drop occurs for $T/T_c^x \sim 1.5$. In the close vicinity of these reduced temperatures, the masses of the physical σ and f_0 anticross and the nonstrange-strange $\sigma_{NS} - \sigma_S$ system masses cross Fig.5(b). It means that after anticrossing the physical σ becomes identical with pure strange quark system σ_S while the physical

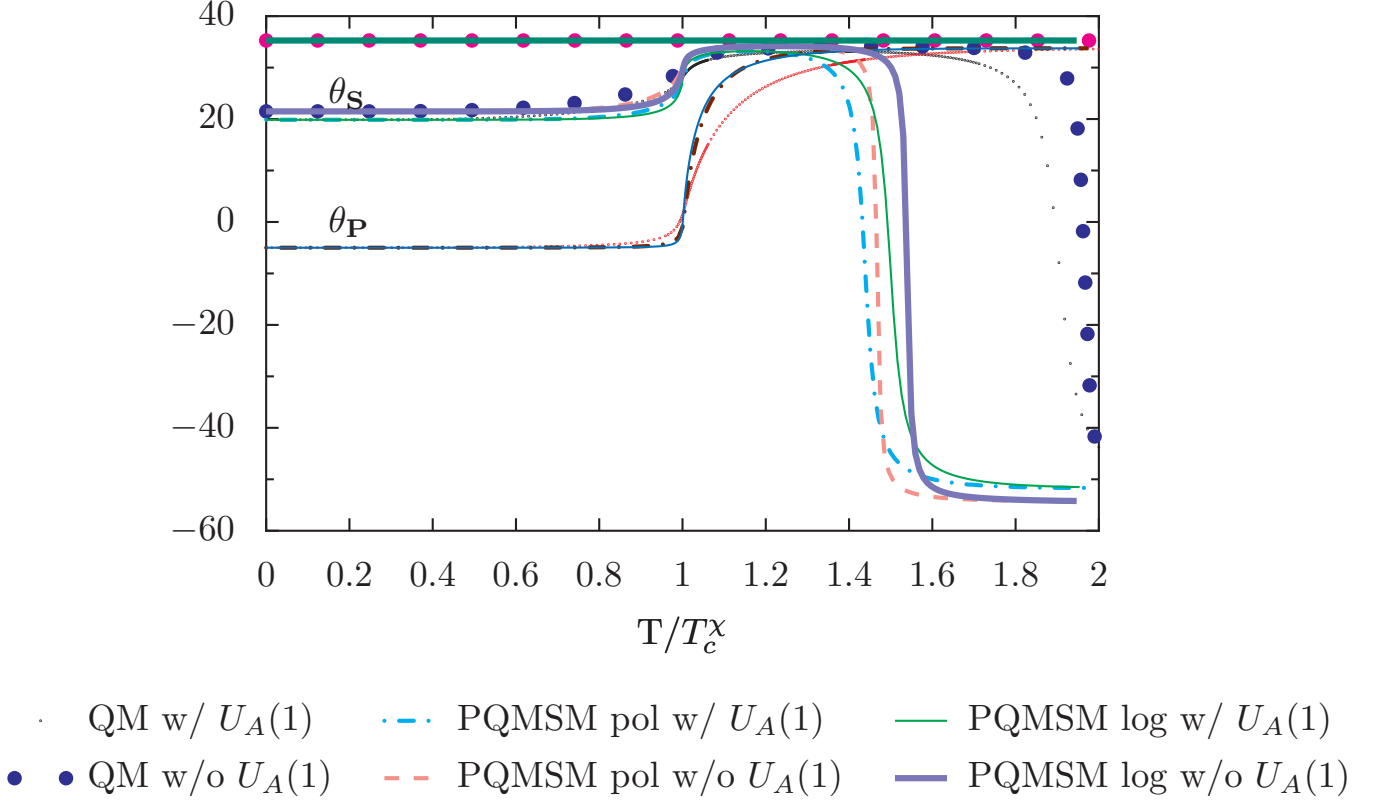


FIG. 4: The scalar θ_s and pseudoscalar θ_p mixing angle variations with respect to the reduced temperature at zero chemical potential are plotted. We have given the plots for QMS, PQMS:log and PQMS:pol models considering the cases in the presence as well as absence of axial $U_A(1)$ explicit symmetry breaking term. The dotted lines show the result with anomaly in QMS model while the solid big dot lines show the result without anomaly. In PQMS:log model, thick solid lines represent the variations without anomaly while thin solid lines show the result with anomaly. Dash dotted lines are the variations with anomaly in PQMS:pol model, while dash lines are the corresponding results in the absence of anomaly.

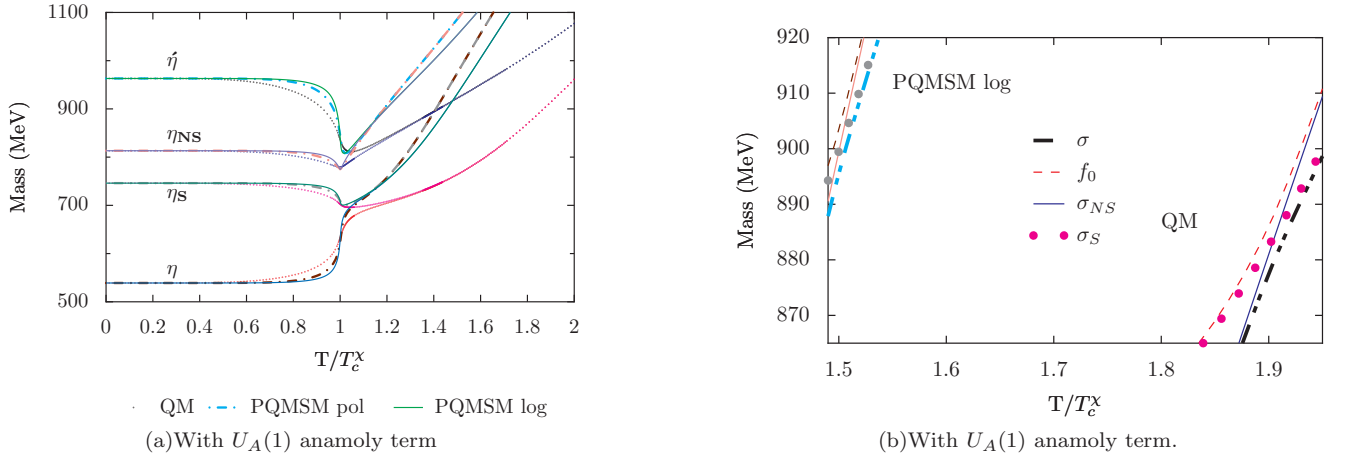


FIG. 5: Fig.5(a) shows the mass variations for the physical η , η' and the nonstrange-strange η_{NS} , η_S complex, on the reduced temperature scale. The masses of the physical σ and f_0 anticross and the nonstrange-strange $\sigma_{NS} - \sigma_S$ system masses cross in Fig.5(b).

f_0 becomes degenerate with the pure nonstrange quark system σ_{NS} . Similar drop for the calculations without anomaly happens at a little higher value on the reduced temperature scale in respective models, it occurs around $T/T_c^x \sim 1.95$ in QMS model and around $T/T_c^x \sim 1.6$ in PQMS:log model.

VI. SUMMARY AND DISCUSSION

We have calculated the meson masses and mixing angles for the scalar and pseudoscalar sector in the framework of generalized $2 + 1$ flavour Polyakov loop augmented Quark Meson Linear Sigma (PQMS) Model. The calculation has been done for two different forms of effective Polyakov loop potential, namely the polynomial potential and logarithmic potential and the results have been compared on the reduced temperature scale.

The temperature dependence of nonstrange, strange condensates and Polyakov loop field Φ at zero chemical potential has been calculated from the gap equation in the QMS and PQMS models. Comparison of pseudocritical temperatures calculated from the inflection points of these order parameters indicates, that the chiral transition gets shifted to the higher temperatures as a result of the inclusion of Polyakov loop in the QMS model. We further observe that the variation of the nonstrange condensate in the $T/T_c^x = 0.7$ to 1.5 range becomes sharp in the Polyakov loop augmented QMS models when comparison is made with the pure QMS model calculations. The logarithmic potential for the Polyakov loop produces the sharpest chiral crossover transition in the nonstrange sector. The presence of Polyakov loop potential in QMS model, generates a significant melting of the strange condensate. We infer from the curves in PQMS models that the inclusion of Polyakov loop in QMS model together with the presence of axial anomaly, triggers an early and significant melting of the strange condensate. The earlier melting of the strange condensate in PQMS models in comparison to the pure QMS model result, indicates an early set up of the $U_A(1)$ restoration trend on the relative temperature scale, in the PQMS models.

The mass degeneration of chiral partners (σ , π) and (a_0 , η') in the close vicinity of reduced temperature $T/T_c^x = 1$, is a little diffused in pure QMS model while in the Polyakov augmented PQMS models, this mass degeneration occurs almost exactly at $T/T_c^x = 1$. Further the sharpest variation in the masses is noticed for the PQMS:log model while the PQMS:pol model results also show sharper variation in comparison to the pure QMS model mass variations. This sharpening of the mass variations in the small neighbourhood of $T/T_c^x = 1$ results due to the stronger and sharper melting of the nonstrange condensate triggered by the presence of Polyakov loop potential in the QMS model. Thus we can corroborate also from the behaviour of the chiral partners that the net effect of the Polyakov loop inclusion

in the QMS model, is to make a sharper occurrence of chiral $SU_L(2) \times SU_R(2)$ symmetry restoration transition in the nonstrange sector (almost exactly at the reduced temperature $T/T_c^x = 1$) which is a smooth crossover in pure QMS model. Further, the mass degeneration of chiral partners (K , κ) with η does not occur when the value of the reduced temperature is equal to one, it sets up early in the two PQMS models at $T/T_c^x = 1.3$ while it occurs at $T/T_c^x = 1.5$ in the pure QMS model.

In the two PQMS models, the intersection point of the f_0 and η masses, occurs early when the reduced temperature $T/T_c^x = 1.4$ while in pure QMS model this intersection point is found at $T/T_c^x = 1.7$. This trend of mass degeneration emerges, again as a result of the sharper and stronger melting of the strange condensate in the influence of the Polyakov loop potential in the PQMS models.

The $U_A(1)$ breaking anomaly effect that leads to the mass gap between the two sets of the chiral partners, (σ , π) and (a_0 , η') i.e. $m_\pi = m_\sigma < m_{a_0} = m_{\eta'}$ for $T/T_c^x > 1$, is proportional to the strange condensate σ_y . Since the melting of the strange condensate is stronger and sharper in the Polyakov loop augmented PQMS models, the convergence in the masses of the two sets of chiral partners will be enhanced in these models. The inclusion of Polyakov loop potential in the PQMS models also effects an early set up of $U_A(1)$ restoration trend on the reduced temperature scale. Thus the $U_A(1)$ restoration in PQMS models will finally occur at smaller value of the reduced temperature when a comparison is made with QMS model result.

The smooth approach of the pseudoscalar mixing angle θ_p towards the ideal mixing in QMS model, becomes sharp in the two PQMS models due to the influence of Polyakov loop potential. Further, in comparison to QMS model results, the ideal mixing on the reduced temperature scale is achieved a little earlier in the PQMS models. The θ_s around $T/T_c^x = 1$ grows to its ideal value but for higher temperatures on the reduced temperature scale, in the chirally symmetric phase, the scalar mixing angle drops down to $\theta_s \sim -51^\circ$. In the presence of $U_A(1)$ symmetry breaking term, this drop happens in the QMS model for $T/T_c^x \sim 1.85$ and in the PQMS:log model, the similar drop occurs for $T/T_c^x \sim 1.5$. In the close vicinity of these reduced temperatures, the masses of the physical σ and f_0 anticross and the nonstrange-strange $\sigma_{NS} - \sigma_S$ system masses cross.

Acknowledgments

We are very thankful to Ajit Mohan Srivastava, Tamal K. Mukherjee and Neelima Agarwal for valuable discussions. We acknowledge the support of the Department of Atomic Energy- Board of Research in Nuclear Sciences (DAE-BRNS), India, under the research grant No. 2008/37/13/BRNS. We also acknowledge the computational support of the computing facility which

has been developed by the Nuclear Particle Physics group of the Physics Department. Allahabad University under

the Center of Advanced Studies(CAS) funding of UGC India.

-
- [1] L.D.McLerran, B.Svetitsky, Phys. Rev. **D24**, 450 (1981); B.Svetitsky, Phys. Rep. **132**, 1 (1986).
 - [2] D. H. Rischke, Prog. Part. Nucl. Phys. **52**, 197 (2004).
 - [3] B.Muller, Rep. Prog. Phys. **58**, 611 (1995).
 - [4] A. M. Polyakov, Phys. Lett. **B 72**, 477 (1978).
 - [5] R. D. Pisarski, Phys. Rev. **D 62** 111501(2000).
 - [6] Biswanath Layek, Ananta P. Mishra, Ajit M. Srivastava and Vivek Kumar Tiwari, Phys. Rev. **D 73** 103514 (2006).
 - [7] F. Karsch, Lect. Notes Phys. **583**, 209 (2002).
 - [8] Z. Fodor, S. D. Katz, and K. K. Szabo, Phys. Lett. **B 568**, 73 (2003).
 - [9] C. R. Allton, M. Doering, S. Ejiri, S. J. Hands, O. Kaczmarek, F. Karsch, E Laermann and K. Redlich, Phys. Rev. **D 71**, 054508 (2005).
 - [10] Y. Aoki, Z. Fodor, S. D. Katz and K. K. Szabo, Phys. Lett. **B 643**, 46 (2006).
 - [11] F. Karsch, J. Phys. **G 31**, S633 (2005).
 - [12] F. Karsch, e-Print: arXiv:0701.210 [hep-ph].
 - [13] M. Cheng et al., Phys. Rev. **D 74**, 054507 (2006).
 - [14] M. Cheng et al., Phys. Rev. **D 77**, 014511 (2008).
 - [15] B. J. Schaefer, M. Wagner and J. Wambach, e-Print: arXiv:0910.5628 [hep-ph]
 - [16] B. J. Schaefer, J. M. Pawłowski and J. Wambach, Phys. Rev. **D 76** 074023 (2007)
 - [17] S. Digal, E. Laermann, H. Satz, Eur. Phys. J. **C 18** 583 (2001).
 - [18] Claudia Ratti, Michael A. Thaler and Wolfram Weise, Phys. Rev. **D 73**, 014019 (2006).
 - [19] S. Rößner, C. Ratti, and W. Weise, Phys. Rev. **D 75**, 034007 (2007).
 - [20] S. Rößner, T. Hell, C. Ratti, and W. Weise, Nucl. Phys. **A 814** 118 (2007).
 - [21] S. K. Ghosh, T. K. Mukherjee, M. G. Mustafa and R. Ray, Phys. Rev. **D 73**, 114007 (2006).
 - [22] C. Sasaki, B. Friman and K. Redlich, Phys. Rev **D 75**, 074013 (2003).
 - [23] T. Hell, S. Rößner, M. Cristoforetti and W. Weise, Phys. Rev **D 79**, 014022 (2008).
 - [24] H. Abuki, R. Anglani, R. Gatto, G. Nardulli and M. Ruggieri, Phys. Rev **D 78**, 034034 (2008).
 - [25] M. Ciminale, R. Gatto, N. D. Ippolito, G. Nardulli and M. Ruggieri, Phys. Rev **D 77**, 054023 (2007).
 - [26] W.-J. Fu, Z. Zhang and Y.-X. Liu, Phys. Rev **D 77**, 014006 (2007).
 - [27] K. Fukushima, Phys. Rev **D 77**, 114028 (2008).
 - [28] K. Fukushima, Phys. Rev **D 78**, 114019 (2008).
 - [29] K. Fukushima, Phys. Rev **D 79**, 074015 (2009).
 - [30] H. Hansen, W. M. Alberico, A. Beraudo, A. Molinari, M. Nardi and C. Ratti Phys. Rev. **D 75**, 065004 (2007).
 - [31] P. Costa, M. C. Ruivo, C. A. de Sousa, H. Hansen and W. M. Alberico Phys. Rev. **D 79**, 116003 (2009).
 - [32] P. Costa, M. C. Ruivo, C. A. de Sousa and Yu L. Kalinovsky Phys. Rev. **D 71**, 116002 (2005).
 - [33] P. Costa, M. C. Ruivo, C. A. de Sousa and Yu L. Kalinovsky Phys. Rev. **D 70**, 116013 (2004).
 - [34] B. J. Schaefer and J. Wambach, Phys. Rev. **D 75** 085015 (2007)
 - [35] O. Scavenius, A. Mocsy, I. N. Mishustin, D. H. Rischke, Phys. Rev. **C 64**, 045202 (2001).
 - [36] J. S. Bielich, Phys. Rev. Lett. **84**, 15 (2000).
 - [37] J. T. Lenaghan, D. H. Rischke and J. S. Bielich, Phys. Rev **D 62**, 085008 (2000).
 - [38] G. 'tHooft, Phys. Rev. Lett. **37**, 8 (1976); Phys. Rev **D 14**, 3432 (1976).
 - [39] K. Fukushima, K. Ohnishi, K. Ohta, Phys. Rev **C 63**, 045203 (2001).
 - [40] B. J. Schaefer and M. Wagner, arXiv:0812.2855 [hep-ph].
 - [41] B. J. Schaefer and M. Wagner, Phys. Rev. **D 79** 014018 (2009).
 - [42] Hong Mao, Jinshuang Jin and Mei Huang, e-Print: arXiv:0906.1324 [hep-ph]
 - [43] K. Fukushima, Phys. Lett. **B 591** 277 (2004).
 - [44] Finite Temperature Field Theory Principles and Applications, J. I. Kapusta and C. Gales, Cambridge University Press. citetHooft:78npb
 - [45] G. 't Hooft, Nucl. Phys. **B 138**, 1 (1978).
 - [46] S. Weinberg Phys. Rev. **D 11**, 3583 (1975).